communications physics

ARTICLE

https://doi.org/10.1038/s42005-021-00586-4 OPEN

Two-plasmon spontaneous emission from a nonlocal epsilon-near-zero material

Futai Hu[1], Liu Li[1], Yuan Liu[1], Yuan Meng[1], Mali Gong[1,2]✉ & Yuanmu Yang[1]✉

Plasmonic cavities can provide deep subwavelength light confinement, opening up new avenues for enhancing the spontaneous emission process towards both classical and quantum optical applications. Conventionally, light cannot be directly emitted from the plasmonic metal itself. Here, we explore the large field confinement and slow-light effect near the epsilon-near-zero (ENZ) frequency of the light-emitting material itself, to greatly enhance the "forbidden" two-plasmon spontaneous emission (2PSE) process. Using degenerately-doped InSb as the plasmonic material and emitter simultaneously, we theoretically show that the 2PSE lifetime can be reduced from tens of milliseconds to several nanoseconds, comparable to the one-photon emission rate. Furthermore, we show that the optical nonlocality may largely govern the optical response of the ultrathin ENZ film. Efficient 2PSE from a doped semiconductor film may provide a pathway towards on-chip entangled light sources, with an emission wavelength and bandwidth widely tunable in the mid-infrared.

[1] State Key Laboratory of Precision Measurement Technology and Instruments, Department of Precision Instrument, Tsinghua University, Beijing, China. [2] State Key Laboratory of Tribology, Department of Mechanical Engineering, Tsinghua University, Beijing, China. ✉email: gongml@mail.tsinghua.edu.cn; ymyang@tsinghua.edu.cn

Plasmonics is a burgeoning field of research that exploits the light-matter interaction in metallic nanostructures[1,2]. Recently, there has been a growing interest in quantum plasmonic devices[1,2] for demonstrating wave-particle duality[3], quantum interference[4,5], and quantum entanglement[6,7], using surface plasmon polaritons (SPPs). Quantum plasmonic circuitry requires the development of efficient quantum plasmonic sources[1]. The generation of single- or entangled-SPP can be done either by using the combination of external quantum sources and SPP couplers[6–8], or by the emission of SPPs from quantum sources, such as colloidal quantum dots[9–11], that is directly coupled to a plasmonic cavity. The former approach may suffer from the limited efficiency of the external source and the SPP coupler. For the latter approach, the spatial separation between the emitter and the plasmonic cavity may pose a fundamental limit on the enhancement of the emission rate[9,10]. It remains a grand challenge to generate single- or entangled-SPPs directly from the plasmonic metal.

Two-photon emission (TPE) refers to the simultaneous emission of two photons during a radiative transition process[12–18]. Recent researches suggest TPE as a promising approach to generate entangled photon pairs in semiconductors, as it emits two photons with intrinsic energy conservation and time concurrence[19,20]. Compared to spontaneous parametric down-conversion, a prevailing method to generate entangled photons, TPE does not have the restriction on phase matching and can have 3-order-of-magnitude higher occurrence probability[21–23]. TPE can also occur in a wide temperature range, unlike semiconductor quantum dots that strictly require cryogenic operation[24–26]. In addition, while the typical one-photon emission (OPE) process emits photons with energy above the material bandgap, the TPE spectrum can be extremely broad starting from near-zero frequencies. This indicates that TPE has the potential to provide emission and gain spectrum with an ultra-broad bandwidth not restricted by the material bandgap[19]. However, as a second-order quantum transition, the TPE process has an emission rate typically 5–10 orders-of-magnitude lower than the OPE rate, thus has typically been considered a “forbidden” process. In semiconductors, the low TPE rate is mainly due to the mismatch between the characteristic emitter size and the light wavelength[21,27], as well as the discrepancy between the electron velocity and the group velocity of light.

Due to the spectral separation of OPE and TPE, the TPE rate may be selectively enhanced by the Purcell effect. Previous researchers have demonstrated enhancements of the TPE rate in semiconductors by coupling emitters to a plasmonic bowtie nanoantenna array[14]. However, the experimentally estimated TPE intensity is enhanced by 3 orders of magnitude, still much lower than the OPE rate. This is likely because the optical field is only enhanced in the vicinity of the antenna tip. In addition, the spontaneous emission enhancement near semiconductor emitters is limited by the relatively low quality- (Q-) factor of the antenna resonance. Recently, Rivera et al. theoretically proposed alternative approaches to enhance the TPE rate by placing an atomic emitter near a single-layer graphene that supports SPPs[28], or a polar dielectric film that supports surface phonon polaritons (SPhPs)[29]. More recently, Y. Muniz et al. proposed a similar approach by placing an atomic emitter near thin plasmonic nanostructures[18]. However, a spatial separation between emitters and the field maximum still pose a limit to the overall TPE rate. An integrated light-emitting scheme that is straightforward for the experimental implementation is yet identified. Furthermore, the nonlocal effect, which may significantly change the optical response of ultrathin films supporting SPPs or SPhPs, needs to be carefully considered when dealing with polariton propagation with a large wavevector. Rivera et al. considered the nonlocal correction of TPE near graphene using the zero-temperature random phase approximation[28]. Gonçalves et al. considered the nonlocal correction of TPE near a jellium metal using the d-parameter framework[30].

Here, we propose a scheme to achieve efficient two-plasmon spontaneous emission (2PSE), by employing a degenerately doped semiconductor thin film that simultaneously serves as the light-emitting medium and the plasmonic cavity. Doped semiconductors are known to support SPP modes in the mid- and far-infrared[31]. In this work, we design the epsilon-near-zero (ENZ)[32–39] frequency ω_{ENZ} of the semiconductor film to be around half of its OPE frequency, thus allowing the selective enhancement of the 2PSE rate. Using degenerately doped InSb as a prototype material, a remarkable Purcell factor up to 1.33×10^5 is obtained due to the high field confinement and the slow-light effect[40–42] near its ω_{ENZ}. The nonlocal effect that governs the optical response of the thin film near its ω_{ENZ} is considered using a hydrodynamic model. We show that the 2PSE lifetime can be reduced from tens of millisecond to tens of nanoseconds, making the 2PSE rate comparable to the OPE rate. In addition, the 2PSE spectral peak can be flexibly tuned by varying the doping density of the InSb film.

Results

Model. Our proposed structure consists of a 50-nm-thick degenerately doped InSb film sandwiched between two AlSb layers, as depicted in Fig. 1a. The bottom AlSb layer can serve as a buffer layer between GaAs and InSb[43]. It can also serve as a

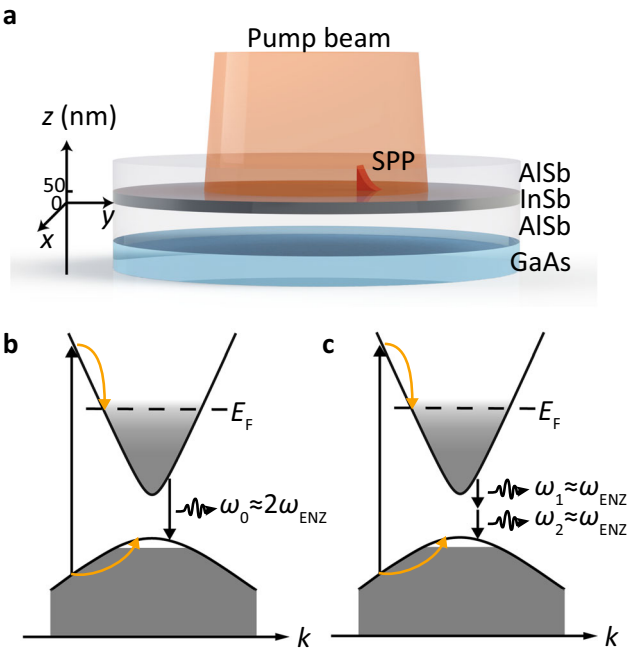

Fig. 1 Schematic of two-plasmon spontaneous emission from a degenerately doped InSb thin film. a Schematics of the proposed structure that supports surface plasmon polaritons (SPPs). **b** Schematics of the one-photon emission process in a semiconductor with a degenerate doping level. The dashed line marks the Fermi level E_F. Yellow arrows represent the thermalization of photoexcited carriers. ω_0 represents the angular frequency of the photon emitted during one-photon emission. ω_{ENZ} is the angular frequency where the permittivity of InSb approaches zero. k is the electron wavevector. **c** Schematics of the two-plasmon spontaneous emission process in a semiconductor with a degenerate doping level. ω_1 and ω_2 represent the angular frequencies of the two plasmons emitted in the spontaneous emission process, respectively.

wide-bandgap barrier to trap the photoexcited carriers in InSb[44]. This layered structure supports SPPs at both AlSb–InSb interfaces at frequencies below ω_{ENZ} of doped InSb. With the deep-subwavelength thickness of the InSb layer, SPPs at both interfaces couple and split into the long range-SPP (LR-SPP) and the short range-SPP (SR-SPP)[45]. Meanwhile, the doped InSb layer may also serve as the light-emitting material through the radiative transition from its conduction band to the valence band (see Supplementary Note 1 for the model of the electronic band structure). With its narrow band gap of 0.17 eV after doping, one may design the OPE frequency of the doped InSb thin film to be about twice its ω_{ENZ}, to selectively enhance the 2PSE rate. Figure 1b, c shows the schematics of the OPE and 2PSE process in the doped InSb thin film. In the initial calculation, we choose a carrier concentration N_e of $6\times10^{18}\,cm^{-3}$ for InSb and a photoexcited carrier density of $1\times10^{14}\,cm^{-3}$. The photoexcited carrier density is set to be much smaller than the carrier concentration, such that the electron temperature remains unchanged, and only the linear permittivity of InSb needs to be considered.

In the local response approximation (LRA), the permittivity of InSb ε is independent of the wavevector of light, and is described by the Drude model as,

$$\varepsilon(\omega)=\varepsilon_\infty-\frac{\omega_p^2}{\omega^2+i\omega\gamma} \tag{1}$$

where ε_∞ is the high-frequency permittivity, ω is the angular frequency, ω_p is the plasma frequency, and γ is the Drude scattering rate. Following the Gauss's law $\varepsilon\nabla\cdot\mathbf{E}=0$, the condition of transverse waves $\nabla\cdot\mathbf{E}=0$ persists unless $\varepsilon=0$. Therefore, SPPs are conventionally treated as transverse waves except at ω_{ENZ}. The permittivity of transverse waves $\varepsilon_T(\omega)$ is thus equal to the local permittivity $\varepsilon(\omega)$, and is plotted in Fig. 2a, with an ENZ energy of 0.105 eV. Figure 2b illustrates the dispersion relation q-Re(ω_q) of the layered structure with LRA, where q is the wavevector along the x–y plane. The density of states (DOS) for SPP modes at a given ω is inversely proportional to the slope of the dispersion curve, i.e., $dq/dRe(\omega_q)$[46]. The dispersion of LR-SPP modes in the thin film, also known as ENZ modes[47], is extremely flat, giving rise to a large DOS near ω_{ENZ}. Figure 2c plots the field confinement factor as a function of q in LRA. Here, the field confinement factor L_q/λ_q is related to the modal length L_q and the modal wavelength λ_q with L_q defined as,

$$L_q=\frac{\int dz\mathrm{Re}[\partial(\omega_q\varepsilon)/\partial\omega_q]|E(z)|^2}{\max\left\{\mathrm{Re}[\partial(\omega_q\varepsilon)/\partial\omega_q]|E(z)|^2\right\}} \tag{2}$$

The dispersion curve is extended to infinity in LRA, with a singularity of DOS and field confinement at large wavevectors. To resolve the singularity issue, which leads to an unphysical, diverging Purcell enhancement, we further consider the nonlocal effect in the InSb thin film[38]. In the nonlocal response approximation (NLRA), SPPs are coupled modes of transverse electromagnetic excitations and longitudinal plasmons. Longitudinal plasmons are collective electron oscillations and hold a distinct dielectric response compared to transverse electromagnetic excitations. Its permittivity ε_L can be described by a hydrodynamic model, and is related to the wavevector of longitudinal plasmons k_L as[45,48,49],

$$\varepsilon_L(\omega,k_L)=\varepsilon_\infty-\frac{\omega_p^2}{\omega^2+i\omega\gamma-\xi^2k_L^2} \tag{3}$$

The k-dependence of permittivity corresponds to the nonlocal effect, and ξ^2 is the nonlocal parameter. Here, we adopt $\xi^2=\left(\frac{3}{5}-i\frac{4}{15}\frac{\gamma}{\omega}\right)v_F^2$ with v_F the Fermi velocity, which is derived from a viscoelastic fluid model for semiconductor films and agrees well with experiments[49,50]. When $k_L^2=(\omega^2+i\gamma\omega-\omega_p^2/\varepsilon_\infty)/\xi^2$, ε_L is equal to zero and $\nabla\cdot\mathbf{E}=0$ is not required, thereby yielding longitudinal plasmons in the InSb film.

Figure 2d depicts the dispersion relation of SPP with NLRA. In the low-q region, dispersion relations with LRA and NLRA are almost identical, which suggests that LRA and NLRA only differ for large in-plane wavevectors (see Methods and Supplementary Note 2 for details). Compared to the dispersion relation with LRA, the nonlocal effect leads to a blue-shift of the SPP modal frequency and a cut-off in-plane wavevector since SPPs only exist below ω_{ENZ}. The singularity of DOS for SPP modes is consequently eliminated. In addition, the cut-off wavevector at ω_{ENZ} is still below ω/v_F. Therefore, the Landau damping effect can be ignored[51,52]. As shown in Fig. 2e, field confinement quickly drops for extremely large in-plane wavevectors, due to the field screening caused by longitudinal waves[45]. Nevertheless, with the nonlocal effect considered, SPP modes in the InSb film can

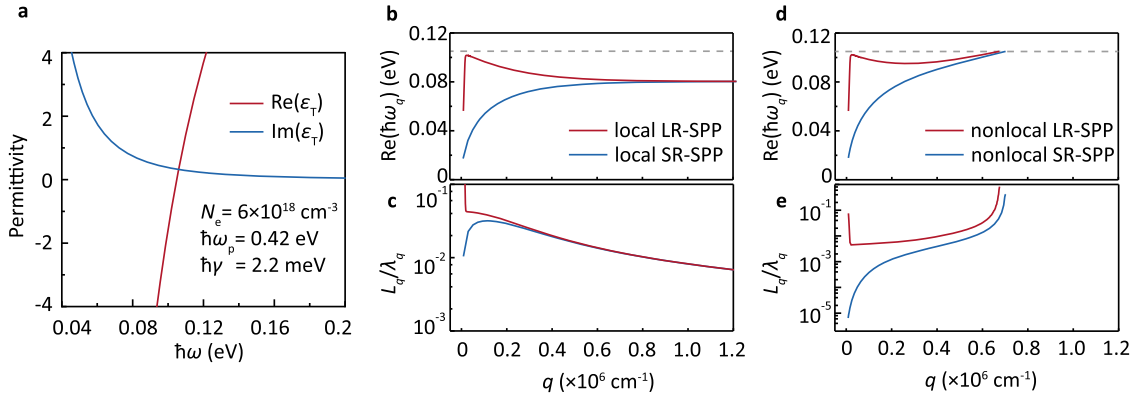

Fig. 2 Dispersion relation and nonlocal effect. a The local permittivity of InSb ε_T with a carrier concentration N_e of $6\times10^{18}\,cm^{-3}$. Here, $\hbar$ is the reduced Planck constant, ω_P is the plasma frequency, γ is the Drude damping rate. **b**–**c** Dispersion relations (**b**) and field confinement factor L_q/λ_q (**c**) of the the long-range surface plasmon polariton (LR-SPP) and the short-range surface plasmon polariton (SR-SPP) modes under the local-response assumption, respectively. Here, q is the in-plane momentum of the SPP. $\hbar\omega_q$ is the modal energy, L_q is the modal length, and λ_q is the modal wavelength. The gray dashed line represents the epsilon-near-zero (ENZ) energy. **d**–**e** Dispersion relations (**d**) and field confinement factor (**e**) of the LR-SPP and SR-SPP modes under the nonlocal-response assumption, respectively.

still retain deep subwavelength confinement, which is critical for the enhancement of the 2PSE rate.

Calculated Purcell enhancement and 2PSE rate. We quantize SPPs using the modal expansion method tailored for a nonlocal plasmonic material, with the material loss included in the complex modal frequency[46], the material dispersion considered in the Brillouin energy density formula[53,54], and the material nonlocality incorporated in Maxwell's equations[45,48,55]. Our modified modal expansion method can prevent a divergent decay rate caused by the unphysically flat dispersion relation and by the breakdown of the dipole approximation when the field is highly concentrated near the emitter. Based on the modal expansion method, we can express the Purcell factor as an integration of the q-resolved Purcell factor f,

$$F(\omega, z) = \int f(q, \omega, z) dq \tag{4}$$

The explicit expression of $f(q, \omega, z)$ is given in Supplementary Note 3.

Electron–hole pairs may form either in-plane dipoles that can be excited by the in-plane electric field $E_{x\text{-}y}$ or out-of-plane dipoles that can be excited by the out-of-plane electric field E_z. Figure 3a–d depicts $f(q, \omega)$ contributed by $E_{x\text{-}y}$ and E_z, respectively. The spectral broadening of $f(q, \omega)$ is induced by the imaginary part of the modal frequency[56]. The spectral broadening indicates non-radiative channels related to material losses, giving rise to a high Purcell factor at low frequencies as shown in Fig. 3e, f. This feature is also observed in the Green's function method[16,55]. An enhanced non-radiative decay rate in lossy materials may affect the Purcell enhancement of emitters, which is important in realizing our proposal to enhance the 2PSE process. However, in this work, the enhanced non-radiative decay at low frequencies barely contributes to the 2PSE process. The non-radiative decay related to material losses near the ENZ frequency can be neglected due to the high Q-factor of the SPP mode (~43). We further exclude the non-radiative decay caused by Landau damping by introducing a wavevector cut-off where the modal frequency reaches the ENZ frequency.

At the center of the InSb layer ($z = 25$ nm), due to the parity, $E_{x\text{-}y}$ of LR-SPPs equals to zero, while E_z of SR-SPPs equals to zero. LR-SPPs have a weak spectral broadening, high peak value and flat dispersion compared to SR-SPPs. Out-of-plane dipoles therefore obtain a Purcell factor F up to 1.33×10^5 with a narrow spectral bandwidth, while the Purcell effect for in-plane dipoles is much broader with a lower peak value. At the edge of the InSb film ($z = 3$ nm), LR-SPPs and SR-SPPs can excite both in-plane and out-of-plane dipoles. For in-plane dipoles, the Purcell enhancement is stronger and narrower due to the contribution of LR-SPPs. However, for out-of-plane dipoles, the peak Purcell enhancement drops due to the field screening effect near the edge[45,51].

The OPE and 2PSE rates tailored by the Purcell effect can be formulated as[14,29],

$$\begin{aligned} R_{\mathrm{OPE}}(\omega_0) &= F(\omega_0) R^0_{\mathrm{OPE}}(\omega_0) \\ R_{\mathrm{2PSE}}(\omega_1, \omega_2) &\propto F(\omega_1) F(\omega_2) R^0_{\mathrm{2PSE}}(\omega_1, \omega_2) \end{aligned} \tag{5}$$

where $R^0{}_{\mathrm{OPE}}(\omega_0)$ and $R^0{}_{\mathrm{2PSE}}(\omega_1, \omega_2)$ represent the OPE and 2PSE rates in the vacuum state, respectively (see Supplementary Note 4 for details). The valance band of InSb splits into subbands due to the confinement in the z-direction. Here, we focus on the transition from the conduction (C) band to the heavy-hole (HH) band. There are two 2PSE paths: C_n-HH_n and $C_{n+/-1}$-HH_n, where n is the quantum number of the subband. 2PSE includes one interband transition and one intersubband transition. In the C_n-HH_n transition, both transitions are excited by $E_{x\text{-}y}$, as shown in Fig. 3g. In the $C_{n+/-1}$-HH_n transition, the interband transition is excited by $E_{x\text{-}y}$ and the intersubband transition is excited by E_z, as shown in Fig. 3h.

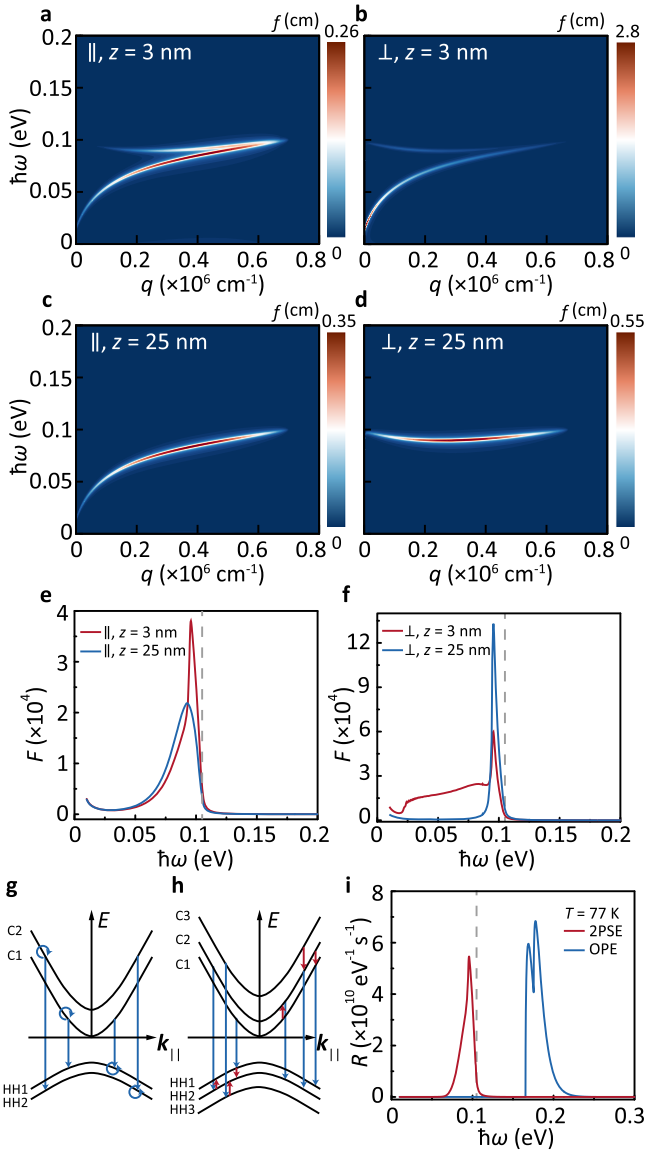

Fig. 3 Purcell effect and two-plasmon spontaneous emission spectra. a–b The q-resolved Purcell factors f as a function of the in-plane momentum q and the energy $\hbar\omega$ for both in-plane (||) and out-of-plane (⊥) dipole orientations at $z = 3$ nm. **c–d** The q-resolved Purcell factors f as a function of q and $\hbar\omega$ for both dipole orientations at $z = 25$ nm. **e–f** The Purcell factor F as a function of $\hbar\omega$ for both dipole orientations. The gray dashed line represents the epsilon-near-zero (ENZ) energy. **g** Two-plasmon spontaneous emission through the C_n-HH_n transition. Here, C represents the conduction subband and HH represents the heavy-hole subband. $\boldsymbol{k}_{||}$ is the the in-plane electron wavevector. The blue arrow represents the transition excited by the in-plane polarization $E_{x\text{-}y}$. **h** Two-plasmon spontaneous emission through the $C_{n+/-1}$-HH_n transition. The blue arrow represents the transition excited by $E_{x\text{-}y}$. The red arrow represents the transition excited by the out-of-plane polarization E_z. **i** The one-photon emission (OPE) and the two-plasmon spontaneous emission (2PSE) rates $R(\hbar\omega)$ in the InSb film averaged over the z-position at an operation temperature $T = 77$ K.

Figure 3i shows the resulting OPE and 2PSE spectra in the InSb film averaged in the z-direction at 77 K. The calculated spectral rate of 2PSE in the InSb film close to its ENZ frequency is comparable to its OPE rate. The ratio of the z-averaged lifetimes between OPE and 2PSE increases from 5.8×10^{-8} in bulk InSb to 0.27, with a 2PSE lifetime of only 2.5 ns. This enhancement is robust at lower temperatures, with a ratio of 0.15 at 30 K and a ratio of 0.03 at 4 K. The current design requires low temperature operation of the two-plasmon emitter, which may be a concern for certain applications.

Discussion

Moreover, while the spectrum of OPE in a semiconductor is generally fixed by the material bandgap, the spectrum of 2PSE in the proposed structure can be flexibly engineered. We further investigate the dependence of the 2PSE spectrum on the carrier density in the InSb film. ω_{ENZ} of InSb can be largely tuned by the carrier concentration N_e. As shown in Fig. 4, with an increasing N_e from 4×10^{18} cm^{-3} to 1×10^{19} cm^{-3}, the spectral peak of 2PSE in InSb can blue-shift by 34%. Besides, the emission bandwidth can be flexibly tuned from 13 to 33 meV. The tuning of N_e can be done by chemical doping or by applying a static electric field. Alternatively, the SPP dispersion can be actively tuned by including additional tunable materials, such as phase-changing vanadium dioxide in the vicinity of the plasmonic cavity[57].

In conclusion, we theoretically show that ultrafast and tunable 2PSE can be realized in a nonlocal ENZ film, by spatially and spectrally matching 2PSE with highly confined SPP modes. Similar concepts can be extended to other semiconductors, 2D materials[58,59], and superconductors supporting Josephson plasmons[60]. The emitted SPP pair have intrinsic time concurrence and energy conservation, which predicts a time-energy entanglement or correlation[61]. TPE also shows the polarization entanglement when eliminating the degeneracy of the heavy-hole and light-hole valence band at the band edge[19]. One of the potential advantages of an entangled light source emitting in the 8–12 μm wavelength range is that it's within an atmospheric window which is desirable for free-space quantum communication[62–64]. The single-photon detection in mid-infrared can be realized using detectors based on either quantum wells[65,66] or superconducting devices[67–69]. The efficient SPP emission can be used for realizing plasmonic amplification and increasing plasmon coherence, two crucial elements in plasmonic circuitry[70,71] and nano-lasing[72]. The generated SPPs can be efficiently coupled to the free space using nanoantennas (see Supplementary Note 5 for details)[73]. In addition, the carrier can potentially be injected by electrical means, with possibilities for further on-chip integration.

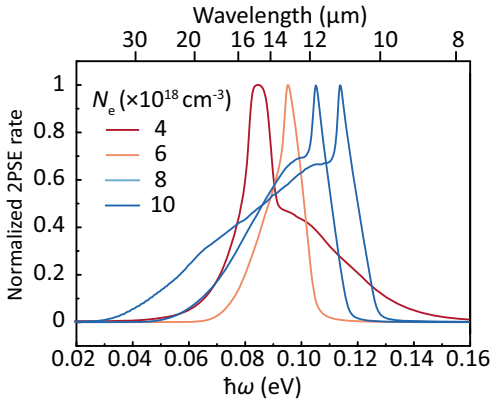

Fig. 4 Two-plasmon spontaneous emission with tunable emission wavelength. Normalized two-plasmon spontaneous emission rate as a function of energy $\hbar\omega$ with different carrier concentration N_e at an operation temperature $T = 77$ K.

Methods

Model of the material permittivity. The linear optical properties of doped semiconductors are mainly governed by the inter-band transition, intra-band transition, and optical phonon absorption[74]. Here we use the same optical properties for both bulk InSb and InSb with a finite thickness. Within the OPE and 2PSE spectra, the inter-band absorption below the Fermi energy is mostly prohibited by Pauli blocking, due to the degenerate doping level in InSb. Meanwhile, since the optical phonon frequency of InSb[75] is relatively far away from ω_{ENZ}, the optical phonon absorption is also ignored here. The Drude model[76] can be written as $\varepsilon = \varepsilon_\infty - \omega_p^2/(\omega^2 + i\gamma\omega)$. The plasma frequency ω_p is given by $\omega_p^2 = N_e e^2/(\varepsilon_0 m_c)$, where m_c is the effective mass of conduction-band electrons. For a given N_e, we can obtain $\gamma = e/(m_c \mu_e)$ and $v_F = \hbar(3\pi^2 N_e)^{1/3}/m_c$, where e is the electron charge, μ_e is the electron mobility[5]. In this work, we assume μ_e to be 11000 cm^2 V^{-1} s^{-1}[77].

Field distribution and dispersion relation. The nonlocality in the metallic film is described by a semiclassical hydrodynamical model[45,48–50]. Here we incorporate longitudinal waves into Maxwell's equations by introducing longitudinal components into the polarization of free electrons. The field distribution can therefore be solved analytically by assuming that transverse waves exponentially decay near the doped InSb/AlSb interface and that longitudinal waves only exist within the InSb layer.

Data availability

The datasets generated during and/or analyzed during the current study are available from the corresponding author on reasonable request.

Code availability

The codes used during the current study are available from the corresponding author on reasonable request.

Received: 1 July 2020; Accepted: 24 March 2021;
Published online: 23 April 2021

References

1. Tame, M. S. et al. Quantum plasmonics. *Nat. Phys.* **9**, 329–340 (2013).
2. Bozhevolnyi, S. I. & Khurgin, J. B. The case for quantum plasmonics. *Nat. Photonics* **11**, 398–400 (2017).
3. Kolesov, R. et al. Wave-particle duality of single surface plasmon polaritons. *Nat. Phys.* **5**, 470–474 (2009).
4. Di Martino, G. et al. Observation of quantum interference in the plasmonic Hong-Ou-Mandel effect. *Phys. Rev. A* **1**, 034004 (2014).
5. Fakonas, J. S., Lee, H., Kelaita, Y. A. & Atwater, H. A. Two-plasmon quantum interference. *Nat. Photonics* **8**, 317–320 (2014).
6. Altewischer, E., Van Exter, M. & Woerdman, J. Plasmon-assisted transmission of entangled photons. *Nature* **418**, 304–306 (2002).
7. Fasel, S., Halder, M., Gisin, N. & Zbinden, H. Quantum superposition and entanglement of mesoscopic plasmons. *N. J. Phys.* **8**, 13 (2006).
8. Tsakmakidis, K. L., Boyd, R. W., Yablonovitch, E. & Zhang, X. Large spontaneous-emission enhancements in metallic nanostructures: towards LEDs faster than lasers. *Opt. Express* **24**, 17916–17927 (2016).
9. Fedutik, Y., Temnov, V., Schöps, O., Woggon, U. & Artemyev, M. Exciton-plasmon-photon conversion in plasmonic nanostructures. *Phys. Rev. Lett.* **99**, 136802 (2007).
10. Falk, A. L. et al. Near-field electrical detection of optical plasmons and single-plasmon sources. *Nat. Phys.* **5**, 475–479 (2009).
11. Tamada, A. et al. Single plasmon generation in an InAs/GaAs quantum dot in a transfer-printed plasmonic microring resonator. *ACS Photonics* **6**, 1106–1110 (2019).
12. He, L.-s & Feng, X.-l Two-photon emission spectrum of a two-level atom in an ideal cavity. *Phys. Rev. A* **49**, 4009 (1994).
13. Lissandrin, F., Saleh, B. E., Sergienko, A. V. & Teich, M. C. Quantum theory of entangled-photon photoemission. *Phys. Rev. B* **69**, 165317 (2004).
14. Nevet, A. et al. Plasmonic nanoantennas for broad-band enhancement of two-photon emission from semiconductors. *Nano Lett.* **10**, 1848–1852 (2010).
15. Lin, Z. & Vučković, J. Enhanced two-photon processes in single quantum dots inside photonic crystal nanocavities. *Phys. Rev. B* **81**, 035301 (2010).

16. Poddubny, A. N., Ginzburg, P., Belov, P. A., Zayats, A. V. & Kivshar, Y. S. Tailoring and enhancing spontaneous two-photon emission using resonant plasmonic nanostructures. *Phys. Rev. A* **86**, 5 (2012).
17. Melzer, S., Ruppert, C., Bristow, A. D. & Betz, M. Stimulated two-photon emission in bulk CdSe. *Opt. Lett.* **43**, 5066–5069 (2018).
18. Muniz, Y., Manjavacas, A., Farina, C., Dalvit, D. & Kort-Kamp, W. Two-photon spontaneous emission in atomically thin plasmonic nanostructures. *Phys. Rev. Lett.* **125**, 033601 (2020).
19. Hayat, A., Nevet, A., Ginzburg, P. & Orenstein, M. Applications of two-photon processes in semiconductor photonic devices: invited review. *Semicond. Sci. Technol.* **26**, 18 (2011).
20. Ota, Y., Iwamoto, S., Kumagai, N. & Arakawa, Y. Spontaneous two-photon emission from a single quantum dot. *Phys. Rev. Lett.* **107**, 233602 (2011).
21. Hayat, A., Ginzburg, P. & Orenstein, M. Observation of two-photon emission from semiconductors. *Nat. Photonics* **2**, 238–241 (2008).
22. Kwiat, P. G. et al. New high-intensity source of polarization-entangled photon pairs. *Phys. Rev. Lett.* **75**, 4337 (1995).
23. Hayat, A., Ginzburg, P. & Orenstein, M. High-rate entanglement source via two-photon emission from semiconductor quantum wells. *Phys. Rev. B* **76**, 4 (2007).
24. Huber, D. et al. Strain-tunable GaAs quantum dot: a nearly dephasing-free source of entangled photon pairs on demand. *Phys. Rev. Lett.* **121**, 033902 (2018).
25. Chen, Y., Zopf, M., Keil, R., Ding, F. & Schmidt, O. G. Highly-efficient extraction of entangled photons from quantum dots using a broadband optical antenna. *Nat. Commun.* **9**, 2994 (2018).
26. Liu, J. et al. A solid-state source of strongly entangled photon pairs with high brightness and indistinguishability. *Nat. Nanotechnol.* **14**, 586–593 (2019).
27. Hayat, A., Ginzburg, P. & Orenstein, M. Measurement and model of the infrared two-photon emission spectrum of GaAs. *Phys. Rev. Lett.* **103**, 023601 (2009).
28. Rivera, N., Kaminer, I., Zhen, B., Joannopoulos, J. D. & Soljačić, M. Shrinking light to allow forbidden transitions on the atomic scale. *Science* **353**, 263–269 (2016).
29. Rivera, N., Rosolen, G., Joannopoulos, J. D., Kaminer, I. & Soljacic, M. Making two-photon processes dominate one-photon processes using mid-IR phonon polaritons. *Proc. Natl Acad. Sci. U.S.A.* **114**, 13607–13612 (2017).
30. Gonçalves, P. et al. Plasmon–emitter interactions at the nanoscale. *Nat. Commun.* **11**, 1–13 (2020).
31. Wagner, M. et al. Ultrafast dynamics of surface plasmons in InAs by time-resolved infrared nanospectroscopy. *Nano Lett.* **14**, 4529–4534 (2014).
32. Alu, A., Silveirinha, M. G., Salandrino, A. & Engheta, N. Epsilon-near-zero metamaterials and electromagnetic sources: tailoring the radiation phase pattern. *Phys. Rev. B* **75**, 155410 (2007).
33. Capretti, A., Wang, Y., Engheta, N. & Dal Negro, L. Comparative study of second-harmonic generation from epsilon-near-zero indium tin oxide and titanium nitride nanolayers excited in the near-infrared spectral range. *ACS Photonics* **2**, 1584–1591 (2015).
34. Liberal, I. & Engheta, N. Near-zero refractive index photonics. *Nat. Photonics* **11**, 149–158 (2017).
35. Reshef, O., De Leon, I., Alam, M. Z. & Boyd, R. W. Nonlinear optical effects in epsilon-near-zero media. *Nat. Rev. Mater.* **4**, 535–551 (2019).
36. Khurgin, J. B. et al. Adiabatic frequency shifting in epsilon-near-zero materials: the role of group velocity. *Optica* **7**, 226–231 (2020).
37. Kinsey, N., DeVault, C., Boltasseva, A. & Shalaev, V. M. Near-zero-index materials for photonics. *Nat. Rev. Mater.* **4**, 742–760 (2019).
38. Yang, Y. et al. Femtosecond optical polarization switching using a cadmium oxide-based perfect absorber. *Nat. Photonics* **11**, 390 (2017).
39. Yang, Y. et al. High-harmonic generation from an epsilon-near-zero material. *Nat. Phys.* **15**, 1022–1026 (2019).
40. Tsakmakidis, K. L., Hess, O., Boyd, R. W. & Zhang, X. Ultraslow waves on the nanoscale. *Science* **358**, eaan5196 (2017).
41. Boyd, R. W. Material slow light and structural slow light: similarities and differences for nonlinear optics. *JOSA B* **28**, A38–A44 (2011).
42. Khurgin, J. B. & Tucker, R. S. *Slow Light: Science and Applications* (CRC Press, 2018).
43. Kang, S. S. et al. High-quality 100 nm thick InSb films grown on GaAs (001) substrates with an InxAl1–xSb continuously graded buffer layer. *lACS Omega* **3**, 14562–14566 (2018).
44. Liu, C., Li, Y. & Zeng, Y. Progress in antimonide based III-V compound semiconductors and devices. *Engineering* **2**, 617 (2010).
45. Moreau, A., Ciraci, C. & Smith, D. R. Impact of nonlocal response on metallodielectric multilayers and optical patch antennas. *Phys. Rev. B* **87**, 045401 (2013).
46. Archambault, A., Teperik, T. V., Marquier, F. & Greffet, J.-J. Surface plasmon Fourier optics. *Phys. Rev. B* **79**, 195414 (2009).
47. Campione, S., Brener, I. & Marquier, F. Theory of epsilon-near-zero modes in ultrathin films. *Phys. Rev. B* **91**, 121408 (2015).
48. Raza, S., Christensen, T., Wubs, M., Bozhevolnyi, S. I. & Mortensen, N. A. Nonlocal response in thin-film waveguides: loss versus nonlocality and breaking of complementarity. *Phys. Rev. B* **88**, 115401 (2013).
49. De Ceglia, D. et al. Viscoelastic optical nonlocality of low-loss epsilon-near-zero nanofilms. *Sci. Rep.* **8**, 9335 (2018).
50. Halevi, P. Hydrodynamic model for the degenerate free-electron gas: generalization to arbitrary frequencies. *Phys. Rev. B* **51**, 7497 (1995).
51. Enoch, S. & Bonod, N. *Plasmonics: From Basics to Advanced Topics.* Vol. 167 (Springer, 2012).
52. Khurgin, J. B. Ultimate limit of field confinement by surface plasmon polaritons. *Faraday Discuss.* **178**, 109–122 (2015).
53. Rivera, N. & Kaminer, I. Light–matter interactions with photonic quasiparticles. *Nat. Rev. Phys.* **2**, 538–561 (2020).
54. Jackson, J. D. *Classical electrodynamics*. 3rd edn (John Wiley & Sons, 1999).
55. Ferreira, B. A., Amorim, B., Chaves, A. & Peres, N. Quantization of graphene plasmons. *Phys. Rev. A* **101**, 033817 (2020).
56. Iwase, H., Englund, D. & Vučković, J. Analysis of the Purcell effect in photonic and plasmonic crystals with losses. *Opt. Express* **18**, 16546–16560 (2010).
57. Folland, T. G. et al. Reconfigurable infrared hyperbolic metasurfaces using phase change materials. *Nat. Commun.* **9**, 4371 (2018).
58. Rana, F., Strait, J. H., Wang, H. & Manolatou, C. Ultrafast carrier recombination and generation rates for plasmon emission and absorption in graphene. *Phys. Rev. B* **84**, 045437 (2011).
59. Kaminer, I. et al. Efficient plasmonic emission by the quantum Čerenkov effect from hot carriers in graphene. *Nat. Commun.* **7**, ncomms11880 (2016).
60. Rajasekaran, S. et al. Parametric amplification of a superconducting plasma wave. *Nat. Phys.* **12**, 1012 (2016).
61. Van Driel, H. M. Semiconductor optics: on the path to entanglement. *Nat. Photonics* **2**, 212 (2008).
62. Manor, H. & Arnon, S. Performance of an optical wireless communication system as a function of wavelength. *Appl. Opt.* **42**, 4285–4294 (2003).
63. Temporão, G. et al. Mid-infrared single-photon counting. *Opt. Lett.* **31**, 1094–1096 (2006).
64. Corrigan, P., Martini, R., Whittaker, E. A. & Bethea, C. Quantum cascade lasers and the Kruse model in free space optical communication. *Opt. Express* **17**, 4355–4359 (2009).
65. Ueda, T., An, Z., Hirakawa, K. & Komiyama, S. Charge-sensitive infrared phototransistors: characterization by an all-cryogenic spectrometer. *J. Appl. Phys.* **103**, 093109 (2008).
66. Ueda, T., An, Z., Hirakawa, K. & Komiyama, S. *Narrow Gap Semiconductors 2007* (Springer, 2008).
67. Verma, V. et al. in Advanced Photon Counting Techniques XIII. 109780N (International Society for Optics and Photonics).
68. Korneev, A., Korneeva, Y., Florya, I., Voronov, B. & Goltsman, G. NbN nanowire superconducting single-photon detector for mid-infrared. *Phys. Procedia* **36**, 72–76 (2012).
69. Santavicca, D. et al. Energy resolution of terahertz single-photon-sensitive bolometric detectors. *Appl. Phys. Lett.* **96**, 083505 (2010).
70. Basov, D. N. & Fogler, M. M. Quantum materials: the quest for ultrafast plasmonics. *Nat. Nanotechnol.* **12**, 187 (2017).
71. Heeres, R. W., Kouwenhoven, L. P. & Zwiller, V. Quantum interference in plasmonic circuits. *Nat. Nanotechnol.* **8**, 719 (2013).
72. Ma, R.-M. & Oulton, R. F. Applications of nanolasers. *Nat. Nanotechnol.* **14**, 12–22 (2019).
73. Bogdanov, S. I. et al. Ultrafast quantum photonics enabled by coupling plasmonic nanocavities to strongly radiative antennas. *Optica* **7**, 463–469 (2020).
74. Amirtharaj, P. M. & Seiler, D. G. *Devices, Measurements, and Properties* 2nd edn, Vol. 2 (McGraw-Hill Professional, 1994).
75. Lockwood, D., Yu, G. & Rowell, N. Optical phonon frequencies and damping in AlAs, GaP, GaAs, InP, InAs and InSb studied by oblique incidence infrared spectroscopy. *Solid State Commun.* **136**, 404–409 (2005).
76. Hofmann, P. *Solid State Physics: an Introduction* (John Wiley & Sons, 2015).
77. Litwin-Staszewska, E., Szymańska, W. & Piotrzkowski, R. The electron mobility and thermoelectric power in InSb at atmospheric and hydrostatic pressures. *Phys. Status Solidi* **106**, 551–559 (1981).

Acknowledgements

This work was supported by the startup funding provided to Y.Y. by Tsinghua University and by the National Natural Science Foundation of China (Grant 61975251).

Author contributions

Y.Y. and F.H. conceived the idea; F.H. designed the structure and finished most calculation; L.L. provided the theoretical analysis for the polarization entanglement; Y.L. helped the calculation of the dispersion relation. Y.M. provided insight into the nonlocal effect. All authors analyzed the numerical data. F.H. and Y.Y. wrote the manuscript. Y.Y. and M.G. supervised the project.

Competing interests
The authors declare no competing interests.

Additional information
Supplementary information The online version contains supplementary material available at https://doi.org/10.1038/s42005-021-00586-4.

Correspondence and requests for materials should be addressed to M.G. or Y.Y.

Reprints and permission information is available at http://www.nature.com/reprints

Publisher's note Springer Nature remains neutral with regard to jurisdictional claims in published maps and institutional affiliations.